nature photonics

LETTERS

PUBLISHED ONLINE: 22 MARCH 2009 | DOI: 10.1038/NPHOTON.2009.29

# Imaging through nonlinear media using digital holography

Christopher Barsi[1], Wenjie Wan[1] and Jason W. Fleischer[1,2]*

**It is well known that one cannot image directly through a nonlinear medium, as intensity-dependent phase changes distort signals as they propagate. Indirect methods can be used[1–6], but none has allowed for the measurement of internal wave mixing and dynamics. Recently, the reconstruction of nonlinear pulse propagation in fibres was demonstrated by generalizing the techniques of digital holography[7,8] to the nonlinear domain[9]. The method involves two steps: (1) recording the total field (both amplitude and phase) exiting a nonlinear medium and (2) numerically back-propagating the wavefunction. Here, we extend this process to two-dimensional spatial beams and experimentally demonstrate it in a self-defocusing photorefractive crystal, giving examples in soliton formation, dispersive radiation and imaging. For known nonlinearity, the technique enables reconstruction of wave dynamics within the medium and suggests new methods of super-resolved imaging, including subwavelength microscopy and lithography. For unknown nonlinearity, the method facilitates modelling and characterization of the optical response.**

Image transmission through nonlinear materials has been studied for over thirty years[1]. Early methods sought to transmit images through turbulent/nonlinear media by means of phase conjugation and four-wave mixing[2–5]. However, backward geometries require a round trip in the nonlinear material[2,3], and forward geometries compete with other nonlinear processes, such as self-focusing, and often require extra processing to remove distortions[4,5]. More recently, incoherent solitons have been used as multimode waveguides[6], but their image quality is limited by intermodal dispersion[1]. Furthermore, all of these techniques obey imaging conditions that ignore (or compensate for) beam propagation within the volume of the medium. These restrictions are unfortunate, as observations of this evolution are vital to understanding the dynamical effects of nonlinearity, such as mode coupling, new frequency generation and modifications to the signal phase. In terms of imaging, this means that all internal wave mixing must be inferred from only the initial and final profiles, where linear optics can be used. Typically, theories of nonlinear beam propagation are tested experimentally in just this fashion: varying known input parameters and comparing measured outputs. With an accurate model of the underlying beam dynamics, however, this process can be reversed, using the measured output and numerically back-propagating the wave dynamics to recover the (unknown) input[9]. In addition, one can image the nonlinear evolution to an arbitrary axial position inside the material and thus reconstruct the field at any intermediate point.

As in linear digital reconstruction[8], the method requires knowledge of the full complex field exiting the sample. The amplitude can be recorded directly in a camera, but the phase requires an interference (holographic) measurement. In the experiments discussed below, the phase was captured with a standard phase-shifting algorithm[10]. For a known propagator, this complex field can then be integrated numerically forwards or backwards. In the linear regime, for example, the field may be reconstructed simply by implementing the Fresnel transformation integral. For nonlinear propagation, this kernel is modified by an intensity-induced change to the phase.

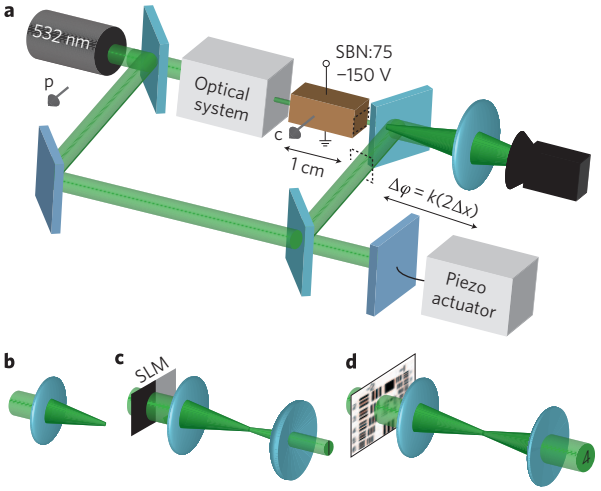


**Figure 1 | Experimental set-up.** Laser light (532 nm), polarized along the crystalline c-axis, is split into two beams. **a**, The object (upper) beam passes through the 'optical system' to generate the input waveform, which is projected onto the crystal. The reference (lower) beam is incremented in phase steps of $\Delta\varphi = \pi/2$; both beams are imaged onto the CCD camera (object planes indicated by dotted lines). **b**–**d**, Different optical systems are used, including a plano-convex lens creating a Gaussian beam (**b**), a spatial light modulator (SLM) producing a $\pi$-stripe (black, 0 rad; grey, $\pi$ rad) (**c**), and a USAF 1951 resolution chart (**d**).

For concreteness, we consider the simplest case of a scalar field undergoing paraxial dynamics. In this approximation, the propagation can be described by the nonlinear Schrödinger equation:

$$\frac{\partial\psi}{\partial z} = \left[i\frac{1}{2k}\nabla_{\perp}^{2} + i\Delta n(|\psi|^2)\right]\psi \equiv \left[D + N(|\psi|^2)\right]\psi \qquad (1)$$

where $\psi(x,y,z)$ is the slowly varying envelope of the field, $k = 2\pi n_0/\lambda$, $\lambda$ is the free-space wavelength, $n_0$ is the medium's base index, $\Delta n(|\psi|^2)$ is the nonlinear index change, and $D$ and $N$ are the linear and nonlinear operators, respectively. A typical choice for $\Delta n(|\psi|^2)$ is the cubic Kerr nonlinearity, with $\Delta n = \gamma|\psi|^2$ where $\gamma$ is the non-linear coefficient. For any nonlinearity, however, issues of invertibility, integrability, vector decoupling and so on, must be considered. Noise and nonlinear instabilities must be examined as well.

[1]Department of Electrical Engineering, Princeton University, Princeton, New Jersey 08544, USA, [2]Program in Applied and Computational Mathematics, Princeton University, Princeton, New Jersey 08544, USA. *e-mail: jasonf@princeton.edu

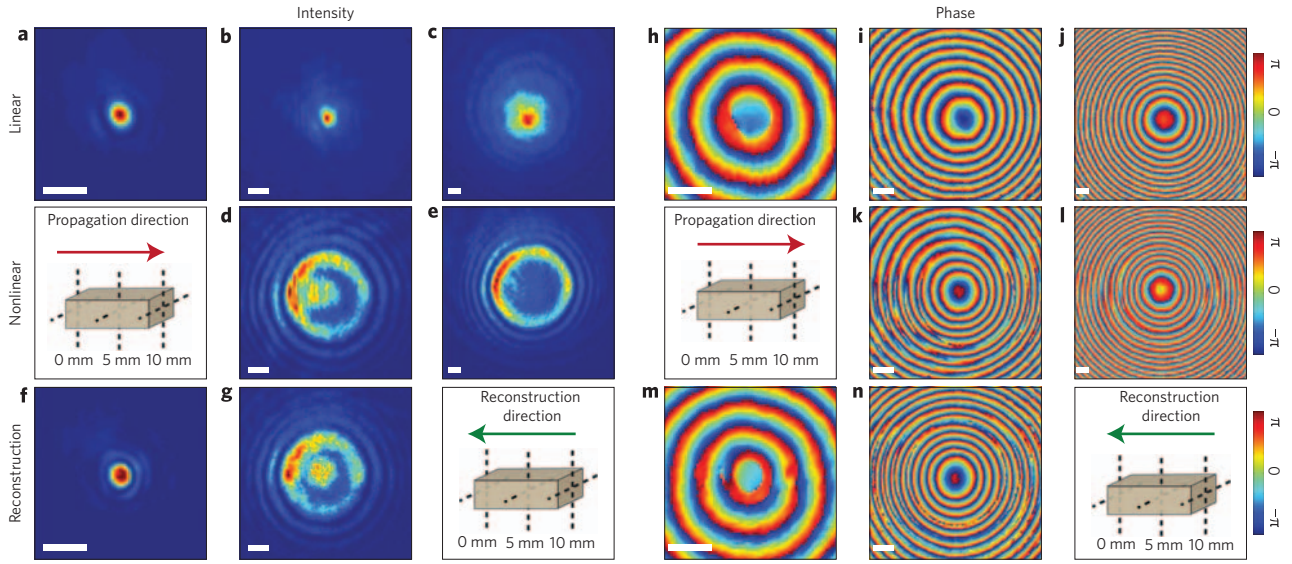


**Figure 2 | Nonlinear digital reconstruction of a self-defocused Gaussian beam.** Left panels: intensity measurements. Right panels: phase measurements, modulo 2π. For both phase and intensity panels: top row, linear measurements; second row, nonlinear measurements; bottom row, numerical reconstructions. From left to right, each column represents 0, 5 and 10 mm distances. Scale bars, 50 μm.

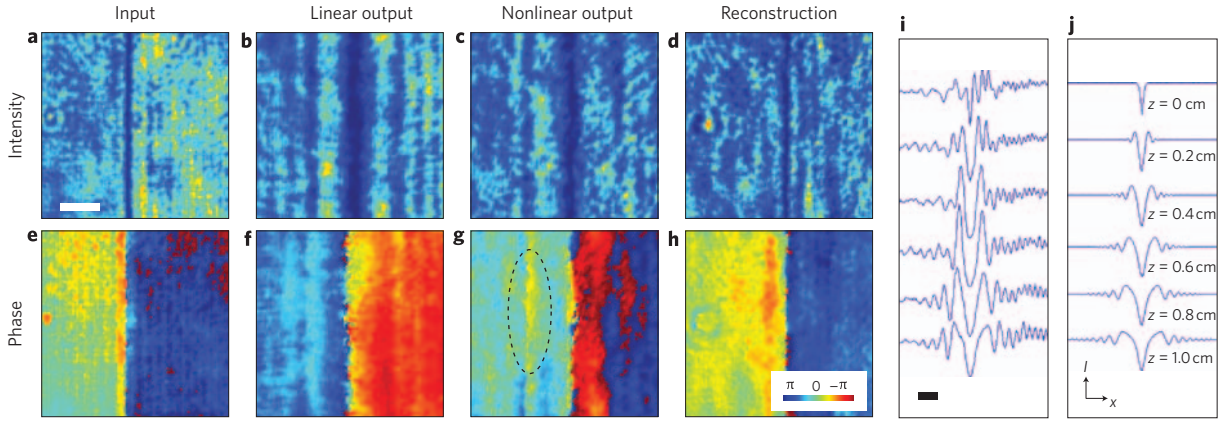


**Figure 3 | Nonlinear reconstruction of evolution of a dark stripe. a–h**, Intensity and phase measurements: experimental input (**a**,**e**), linear output (**b**,**f**), nonlinear output (**c**,**g**), numerically reconstructed input (**d**,**h**). Top row: intensity profile. Bottom row: phase profile, modulo 2π. Scale bar, 50 μm. The dotted oval in **g** indicates appearance of π/2 discontinuity that is successfully eliminated upon reconstruction (**h**). **i**, Reconstruction cross-sections using a backwards propagation algorithm of the internal dynamics of the dark stripe. **j**, Simulation of evolution with 5% intensity noise. Scale bar, 50 μm.

The beam evolution can be calculated numerically using the Fourier split-step method, in which the linear and nonlinear operators act individually for each increment of propagation distance d$z$:

$$\psi(z+\mathrm{d}z) \approx e^{\mathrm{d}z\cdot D} e^{\mathrm{d}z\cdot N(\psi)} \psi(z) \qquad (2)$$

Inverting the equation, that is, applying $\exp(-\mathrm{d}z\cdot N)\exp(-\mathrm{d}z\cdot D)$ to both sides, one can calculate the field at some location $z_i$ given the field farther along the sample at location $z_f > z_i$:

$$\psi(z_i) \approx e^{-\mathrm{d}z\cdot N(\psi)} e^{-\mathrm{d}z\cdot D} \psi(z_f = z_i + \mathrm{d}z) \qquad (3)$$

This back-propagation is essentially an initial-value problem, in which the output is the starting point, and thus will work in situations where inverse scattering may fail, such as media with non-integrable nonlinearities. The method was first demonstrated for one-dimensional pulses in fibre[9] and has undergone much progress in the temporal domain[11,12]. Here, we extend the technique to two-dimensional spatial beams containing image information, emphasizing that the higher dimensionality adds considerable complexity to the inversion, for example, by introducing degenerate solutions or an anisotropic response.

Experiments were performed using a $2 \times 5 \times 10$ mm$^3$ photorefractive strontium barium niobate (SBN:75) crystal with a self-defocusing nonlinearity, produced by applying an electric field of $-750$ V cm$^{-1}$ along the crystalline axis. As illustrated in Fig. 1, different extraordinarily polarized waveforms were projected onto the input face of the crystal, and the complex field at both the input and output faces was measured. The output field was then numerically back-propagated using equation (3) and compared with the measured input field. Technically, the photorefractive screening nonlinearity of this crystal is saturable, with a response $\Delta n \propto r_{ij}\tilde{I}/(1+\tilde{I})$, where $\tilde{I}$ is the intensity $I = |\psi|^2$, normalized to a background (dark current) intensity, and $r_{ij}$ is the appropriate electro-optic coefficient[13,14]. However, recent experiments have shown that for the defocusing parameters considered here, the simpler Kerr nonlinearity $\Delta n = -|\gamma|I$ proves sufficient for

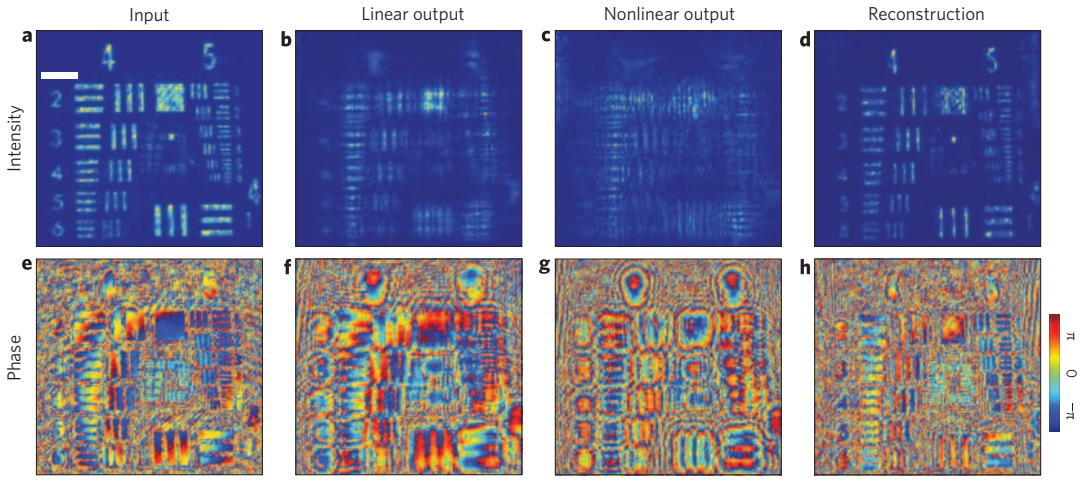


**Figure 4 | Nonlinear digital reconstruction of a self-defocused USAF 1951 resolution chart. a–h**, Intensity and phase measurements: experimental input (**a**,**e**), linear output (**b**,**f**), nonlinear output (**c**,**g**), numerically reconstructed input (**d**,**h**). Top row: intensity profile. Bottom row: phase profile, modulo 2π. Scale bar, 200 μm. Note that the ambiguity that leads to the random phase distribution in the dark regions is caused by the undefined phase there.

modelling[15]. Similarly, loss has been ignored, although the inclusion of linear operators such as absorption should not affect the reconstruction process[9]. On the other hand, the uniaxial nature of the crystal did introduce a slight anisotropy in the nonlinear response; our correction for this is discussed in the Methods section.

To calibrate the algorithm, we first focused a Gaussian beam of ∼10 μW onto the input face of the crystal (Fig. 2a,h). Linear diffraction is shown in Fig. 2b,c,i,j, and nonlinear evolution in Fig. 2d,e,k,l. The dramatically different output in the nonlinear case, particularly after 10 mm of propagation (roughly three diffraction lengths), is shown in Fig. 2e. In particular, the nonlinear beam has a depleted central region and high-frequency fringes at the edges, a profile that cannot occur in the linear case (in which a Gaussian beam stays Gaussian). These features result from wavebreaking of the central portion of the beam into its own tails and are similar to the optical shocks demonstrated in other works[15,16]. This output field was back-propagated numerically to reconstruct the measured input, adjusting the nonlinear coefficient $\gamma$ until the sum-of-squares error between the two profiles was minimized. As shown in Fig. 2f,m there is very good agreement in both phase and intensity with the experimental input. As a check, the experiment was then repeated with the shorter (5 mm) side of the crystal. As shown in Fig. 2d,k and 2g,n, the measured output after 5 mm of propagation matches the reconstruction resulting from back-propagating the 10 mm output halfway. The agreement is particularly pronounced in the asymmetry of the central portion of the beam, which is slightly left of centre. The nonlinear coefficient that was used to generate this reconstruction was then fixed and used for all subsequent experiments.

Although the expanding Gaussian beam experiences significant changes in both intensity and phase, other nonlinear structures, such as solitons, maintain constant-intensity profiles and acquire only an overall phase change upon propagation. Normally, experimental observations of these structures follow from launching a beam close to the initial soliton profile; confirmation is then reported by comparing the original input to the nonlinear output after several diffraction lengths. This observation method, however, says little about evolution towards a steady-state profile, especially for initial conditions far from the soliton existence curve. Cut-back methods provide volumetric information but require crystal damage or special geometry[17]. Other methods, such as near-field probes[18] and scattered-light measurements[17], are similarly direct but work well only for one-dimensional solitons and cross-sections. In contrast, the technique here allows reconstruction, and thus effective imaging, of the beam dynamics all along its propagation, without relying on coupling mechanisms or material modification.

Figure 3 shows such evolution for a dark stripe (generated by a π-shift phase discontinuity) that is initially too narrow, for its intensity, to be a dark soliton. In the linear case (Fig. 3b), the stripe expands to roughly three times its original size. In the nonlinear case (Fig. 3c), the output stripe width has narrowed by ∼30%. Numerical calculations show that this width coincides with the dark soliton width for the experimental parameters, but standard experimental techniques can say nothing more about the beam dynamics. In other words, without showing invariant propagation, the existence of a soliton could not be proved. Here, we use nonlinear digital holography to reconstruct the entire dynamics along the propagation path. As before, the first step is to reconstruct the input (Fig. 3d,h). Note that a phase defect at the output (Fig. 3g) has been eliminated successfully in the reconstruction. In Fig. 3i, we show several cross-sections of the reconstruction at intermediate distances within the crystal. As the beam propagates, the stripe widens to a dark soliton profile, radiating energy as it adjusts. The evolution is complex: the initial noise smoothens, owing to the defocusing nonlinearity, the beam profile becomes more symmetric, diffraction of the central dark stripe is arrested, and the radiated waves self-steepen and form dispersive shock waves[15,16]. Similar profiles have been observed in fibre solitons[19] but have not been demonstrated in the spatial case. Here, we reconstruct the entire dynamics, showing that the central profile settles into its dark soliton form at about 5 mm, whereas the tails need a longer propagation distance to relax. This semi-empirical reconstruction compares favourably with the ideal simulated case, shown in Fig. 3j.

A more complex example is provided by the nonlinear evolution of an Air Force 1951 resolution chart (Fig. 4). In the linear case, the input (Fig. 4a,e) has diffracted considerably (Fig. 4b,f), but the characters are still recognizable. After nonlinear propagation (Fig. 4c,g), however, the original intensity profile has been obliterated almost completely, especially for the numerical symbols, and the phase profile is severely blurred. Nevertheless, there is very good agreement between experimental and reconstructed phase and intensity. There is thus much potential in this technique for physical encryption. As with the dark soliton (Fig. 3f), the reconstruction of the phase is particularly well defined. This is both surprising and fortunate, because the phase is a much more sensitive quantity and typically carries more information[20]. Indeed, from Fig. 4h, it is possible

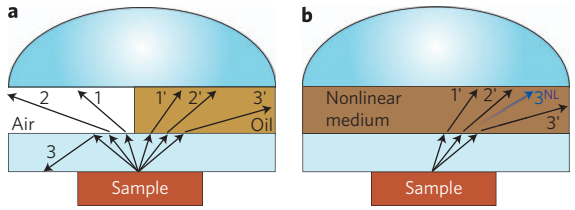


**Figure 5 | Schematic for nonlinear holographic microscopy. a**, Standard linear microscopy cannot capture rays 2 or 3. Index-matching between the sample slide and lens, through oil immersion, for example, allows detection of ray 2′, but ray 3′ still escapes. **b**, With immersion in a nonlinear medium, rays 3′ and 2′ can couple, generating a new (sum) wave, $3^{NL}$, which can be detected. (The difference wave and similar coupling to ray 1′ are not shown.) Through nonlinear digital holography, the original wave 3′ can be reconstructed from the measured ray $3^{NL}$, giving a higher effective numerical aperture.

to resolve the 10 μm bars of the chart, a resolution limited mainly by the non-ideal properties (defects and striations) of the crystal.

The sharpness of the reconstruction highlights an irony inherent in self-defocusing media: nonlinear mode-coupling of high spatial frequencies can lead to focusing effects[21–23]. (Although focusing nonlinearities can also couple these modes, noise-induced instabilities can dominate the signal and may limit the ability to invert equation (2).) The end results are larger effective numerical apertures and finer spatial resolution[24], so that the technique naturally leads to nonlinear extensions of digital microscopy. A simple ray-tracing schematic of this application, in transmission geometry, is shown in Fig. 5. Rays not captured by linear techniques (Fig. 5a) are still not captured in the nonlinear method (Fig. 5c), but information about them can be obtained through their daughter waves. Here, the super-resolution effect results from knowledge of the nonlinear propagation kernel. This allows reconstruction of the dynamics, deconvolution of the wave mixing, and therefore recovery of the underlying (missing) spatial features.

Theoretically, this method can be extended to near-field, subwavelength reconstructions as well. In this case, nonlinear wave mixing would couple evanescent waves with propagating ones (although a more accurate model than equation (1) would be necessary). This method has potential to work follows from recent observations of the Goos–Hänchen effect[25], in which a totally internally reflected beam is spatially translated from the incident beam. This translation, owing to phase shifts of evanescent waves at the interface[26], is normally on the order of a wavelength but can be enhanced significantly by nonlinearity[27–29]. Combined with the reconstruction algorithm, this coupling of near-field behaviour with far-field propagation could be extended to imaging. Moreover, unlike traditional point-by-point scanning techniques[30], the nonlinear digital holography presented here is an inherently wide-angle, far-field form of microscopy. From the opposite perspective, such nonlinear wave mixing could allow subwavelength lithography with super-wavelength-scale initial patterns.

The limits on resolution depend on the underlying nature of the nonlinearity, the quality of the medium and the effects of noise. For example, the photorefractive crystal used above is a poor choice for high-resolution experiments, because the charge transport of its material response is inherently nonlocal. The most serious obstacle is noise, both as a detriment to the signal and as an irreversible source of instability. For example, nonlinear coupling can lead to modulation instabilities, even in defocusing media[21]. On the other hand, we note that nonlinearity leads naturally to optical squeezing, and with the hope that quantum optics can improve upon the classical ideas presented here. The ultimate resolution limits of the technique, therefore, remain to be determined.

In conclusion, we have successfully carried out the digital reconstruction of optical spatial beams propagating in a nonlinear medium. This should prove useful both for basic studies of coupled wave dynamics and for new methods of image/signal processing.

## Methods

To create the input, a wide, collimated beam from a 532 nm Coherent Verdi laser was split into two parts, as shown in Fig. 1. The lower, unmodified beam acted as a plane-wave reference, which was reflected from a mirror with a longitudinal position controlled by a piezo-electric actuator. The upper beam was passed through a different optical system for each of the above experiments to create different object signals. The input/output object beam was combined with the reference beam using a beamsplitter, and the total field was then imaged onto a charge-coupled-device (CCD) camera (520 × 492 array with a pixel size of 9.9 μm). The image was magnified approximately four times with a lens to better resolve the features of the field. To shift the reference beam, the piezo-actuated mirror was stepped in increments of $\lambda/4 \pm 5$ nm. Note that although the imaging lens itself gives rise to a quadratic phase factor, because both reference and object beams are imaged together, no extraneous fringes in the interference pattern are produced.

Details of the object beam generation for each experiment are as follows. For the Gaussian-shock example in Fig. 2, the beam was simply focused onto the input face of the crystal using a 20 cm plano-convex lens. The narrow dark stripe in Fig. 3 was created by imprinting a phase discontinuity onto the object beam with a phase-only spatial light modulator. It was imaged and demagnified eight times with a 4*f* system. Finally, the resolution chart in Fig. 4 was imaged with a 4*f* system as well, with unity magnification.

For the digital reconstruction, the frames recorded by the camera were cropped horizontally, and padded with zeros vertically to create 512 × 512 pixel frames. In this way, the beam propagation code could best make use of the fast Fourier transform (FFT) algorithm in the linear step. The numerical pixel size was matched with the effective (demagnified) camera pixel size, 2.5 μm, and the propagation step size was 65 μm. A decrease in the step size to 20 μm showed no appreciable change in the reconstruction, confirming that numerical convergence had been achieved. Note that, in order to yield the circularly symmetric beam of Fig. 2f, a small anisotropic correction of 7% was included for the index of refraction in the *x*-direction for the linear propagator, that is, in the Fourier domain

$$e^{-i\frac{\lambda\Delta z}{4\pi}\left(\frac{k_x^2}{n_0}+\frac{k_y^2}{n_0}\right)} \rightarrow e^{-i\frac{\lambda\Delta z}{4\pi}\left(\frac{k_x^2}{n_0(1+\delta)}+\frac{k_y^2}{n_0}\right)} \quad (4)$$

where $\delta = 0.07$ and $k_x$ and $k_y$ are the wavevectors for the *x*- and *y*-axis. $\delta$ was held constant, although functional dependence on the intensity did not change the result. This numerical solution affected the Gaussian beam at its focus only. Furthermore, it did not affect the other reconstructions. Therefore, we suspect that this modification becomes necessary for high-intensity, focused beams. Other, more complex, models of the photorefractive nonlinearity that include charge transport and saturation effects were not as successful at recovering the input.

Received 19 October 2008; accepted 23 February 2009; published online 22 March 2009

## References

1. Yariv, A. Three-dimensional pictorial transmission in optical fibers. *Appl. Phys. Lett.* **28,** 88–89 (1976).
2. Yariv, A. Compensation for atmospheric degradation of optical beam transmission by nonlinear optical mixing. *Opt. Commun.* **21,** 49–50 (1977).
3. Fischer, B., Cronin-Golomb, M., White, J. O. & Yariv, A. Real-time phase conjugate window for one-way optical field imaging through a distortion. *Appl. Phys. Lett.* **41,** 141–143 (1982).
4. Khyzniak, A. *et al.* Phase conjugation by degenerate forward four-wave mixing. *J. Opt. Soc. Am. A* **1,** 169–175 (1984).
5. Jones, D. C., Lyuksyutov, S. F. & Solymar, L. Three-wave and four-wave forward phase-conjugate imaging in photorefractive bismuth silicon oxide. *Opt. Lett.* **15,** 935–937 (1990).
6. Kip, D., Anastassiou, C., Eugenieva, E., Christodoulides, D. & Segev, M. Transmission of images through highly nonlinear media by gradient-index lenses formed by incoherent solitons. *Opt. Lett.* **26,** 524–526 (2001).
7. Schnars, U. & Jüptner, W. Direct recording of holograms by a CCD target and numerical reconstruction. *Appl. Opt.* **33,** 179–181 (1994).
8. Schnars, U. & Jüptner, W. P. O. Digital recording and numerical reconstruction of holograms. *J. Meas. Sci. Technol.* **13,** R85–R101 (2002).
9. Tsang, M., Psaltis, D. & Omenetto F. Reverse propagation of femtosecond pulses in optical fibers. *Opt. Lett.* **28,** 1873–1875 (2003).
10. Yamaguchi, I. & Zhang, T. Phase-shifting digital holography. *Opt. Lett.* **22,** 1268–1270 (1997).

11. Goldfarb, G. & Li, G. Demonstration of fibre impairment compensation using split-step infinite-impulse-response filtering method. *Electron. Lett.* **44,** 814–815 (2008).
12. Mateo, E., Zhu, L. & Li, G. Impact of XPM and FWM on the digital implementation of impairment compensation for WDM transmission using backward propagation. *Opt. Express* **16,** 16124–16137 (2008).
13. Segev, M., Valley, G. C., Crosignani, B., Diporto, P. & Yariv, A. Steady-state spatial screening solitons in photorefractive materials with external applied field. *Phys. Rev. Lett.* **73,** 3211–3214 (1994).
14. Christodoulides, D. N. & Carvalho, M. I. Bright, dark and gray spatial soliton states in photorefractive media. *J. Opt. Soc. Am. B* **12,** 1628–1633 (1995).
15. Wan, W., Jia, S. & Fleischer, J. W. Dispersive, superfluid-like shock waves in nonlinear optics. *Nature Phys.* **3,** 46–51 (2007).
16. Ghofraniha, N., Conti, C., Ruocco, G. & Trillo, S. Shocks in nonlocal media. *Phys. Rev. Lett.* **99,** 043903 (2007).
17. Shih, M. *et al.* Two-dimensional steady-state photorefractive screening solitons. *Opt. Lett.* **21,** 324–326 (1996).
18. Linzon, Y. *et al.* Near-field imaging of nonlinear pulse propagation in planar silica waveguides. *Phys. Rev. E* **72,** 066607 (2005).
19. Krökel, D., Halas, N. J., Giuliani, G. & Grischkowsky, D. Dark-pulse propagation in optical fibers. *Phys. Rev. Lett.* **60,** 29–32 (1988).
20. Oppenheim, A. V. & Lim, J. S. The importance of phase in signals. *Proc. IEEE* **69,** 529–541 (1981).
21. Agrawal, G. P. Modulation instability induced by cross-phase modulation. *Phys. Rev. Lett.* **59,** 880–883 (1987).
22. Stentz, A. J., Kauranen, M., Maki, J. J., Agrawal, G. P. & Boyd, R. W. Induced focusing and spatial wave breaking from cross-phase modulation in a self-defocusing medium. *Opt. Lett.* **17,** 19–21 (1992).
23. Hickmann, J. M., Gomes, A. S. L. & de Araújo, C. B. Observation of spatial cross-phase modulation effects in a self-defocusing nonlinear medium. *Phys. Rev. Lett.* **68,** 3547–3550 (1992).
24. Jia, S., Wan, W. & Fleischer, J. W. Forward four-wave mixing with defocusing nonlinearity. *Opt. Lett.* **32,** 1668–1670 (2007).
25. Goos, F. & Hänchen, H. Ein neuer und fundamentaler versuch zur totalreflexion. *Ann. Phys.* **1,** 333–346 (1947).
26. Artmann, K. Berechnung der seitenversetzung des totalreflektierten strahles. *Ann. Phys.* **2,** 87–102 (1947).
27. Tomlinson, W. J., Gordon, J. P., Smith, P. W. & Kaplan, A. E. Reflection of a Gaussian beam at a nonlinear interface. *Appl. Opt.* **21,** 2041–2051 (1982).
28. Emile, O., Galstyan, T., Le Floch, A. & Bretenaker, F. Measurement of the nonlinear Goos–Hänchen effect for Gaussian optical beams. *Phys. Rev. Lett.* **75,** 1511–1513 (1995).
29. Jost, B. M., Al-Rashed, A.-A. R. & Saleh, B. E. A. Observation of the Goos–Hänchen effect in a phase-conjugate mirror. *Phys. Rev. Lett.* **81,** 2233–2235 (1998).
30. Ash, E. A. & Nicholls, G. Super-resolution aperture scanning microscope. *Nature* **237,** 510–512 (1972).


## Acknowledgements

This work was supported by the National Science Foundation, the Department of Energy and the Air Force Office of Scientific Research. C.B. would like to thank the Army Research Office for support through a National Defense Science and Engineering Graduate Fellowship.

## Author contributions

All authors have contributed to this paper and agree to its contents.

## Additional information

Reprints and permission information is available online at http://npg.nature.com/reprintsandpermissions/. Correspondence and requests for materials should be addressed to J.W.F.